INL-JOU--18-50510-Revision-1

Comparative Study of Monolithic Platinum and Iridium as Oxygen-Evolving Anodes during the Electrolytic Reduction of Uranium Oxide in a Molten LiCl-Li2O Electrolyte

Steven D Herrmann, P. K. Tripathy, S. M. Frank, J. A. King

The INL is a
U.S. Department of Energy
National Laboratory
operated by
Battelle Energy Alliance

February 2019

Prepared for the U.S. Department of Energy

Under DOE Idaho Operations Office
Contract DE-AC07-05ID14517

For submission to the Journal of Applied Electrochemistry

Comparative Study of Monolithic Platinum and Iridium as Oxygen-Evolving Anodes during the Electrolytic Reduction of Uranium Oxide in a Molten LiCl-Li_2O Electrolyte

S. D. Herrmann[†]*, P. K. Tripathy[†], S. M. Frank[†], J. A. King[‡]

[†]Pyrochemistry and Molten Salt Systems Department, [‡]Fuel & Experiment Assembly and Development Department

Idaho National Laboratory, P.O. Box 1625, Idaho Falls, Idaho, 83415, USA

*corresponding author, e-mail: Steven.Herrmann@inl.gov

Abstract

A series of four electrolytic reduction runs was performed in molten salt at bench scale to compare the performance characteristics of monolithic platinum and iridium as oxygen-evolving anodes, while simultaneously reducing uranium oxide to metal. In each run 25 g of uranium oxide particulate was loaded into a permeable steel basket, which, in turn, was immersed in a pool of LiCl – 1 wt% Li_2O at 650 °C. Both anodes, each 3 mm in diameter, were suspended vertically in the salt pool, adjacent to the steel cathode basket. The anodes were connected in parallel to separate direct current power supplies with the uranium oxide-loaded basket as the common cathode. A cell voltage (3.1 V) was intermittently applied to the system with both power supplies operating concurrently, effecting the reduction of uranium oxide to uranium metal at the cathode basket and the simultaneous oxidation of oxygen anions in the salt to oxygen gas at each anode. Anode and cathode potentials and currents were recorded to compare the performance of platinum vis-à-vis iridium. After completing the series of runs, both anodes were removed and subjected to dimensional, chemical, and microscopic analyses. Even though the accumulated charges on each anode over the series of four runs were similar, the platinum anode exhibited up to 29% reduction in cross-sectional area compared to less than 3% for the iridium anode.

Keywords

Electrolytic reduction, oxide reduction, uranium oxide, platinum anode, iridium anode, lithium chloride-lithium oxide electrolyte

1 Introduction

An electrolytic reduction process for the conversion of uranium oxide to uranium metal in a molten LiCl-Li_2O electrolyte was originally developed by researchers at Argonne National Laboratory [1]. In a typical operation of this process, uranium oxide (UO_2) particulate is loaded into a permeable steel basket and immersed in molten LiCl at 650 °C with a nominal 1 wt% Li_2O content. An inert anode rod is suspended in the electrolyte adjacent to the basket. A power supply is configured to the anode rod and a center cathode rod, embedded in the particulate loaded basket. The power supply is operated at a sufficient cell potential (nominally 3.1 V) to electrochemically reduce the uranium oxide to uranium metal, thereby liberating oxygen anions from the basket to the molten salt electrolyte. Simultaneously, oxygen anions are oxidized to oxygen gas at the anode, where the gas bubbles rise through the salt and are channeled out of the cell.

A primary application of the electrolytic reduction process is a head-end step in an integrated operation for the recovery of uranium and group uranium/transuranium metals from used nuclear oxide fuels. Specifically, used commercial nuclear oxide fuel, which is ~96% uranium oxide, is separated from its cladding and converted to metal

in the prescribed electrolytic reduction process. Once reduced to metal, the used fuel is amenable to further electrochemical treatment (i.e., electrorefining), from which purified uranium and group uranium/transuranium metal products are recovered [2]. The integration of electrolytic reduction and electrorefining technology for reprocessing used nuclear oxide fuels has been the subject matter of considerable research, performed at various institutions over the last decade [3-10].

The electrolytic reduction process for uranium oxide and used nuclear oxide fuels has been developed utilizing primarily monolithic platinum as an inert anode, because it has exhibited reasonable stability in a LiCl-Li_2O-O_2 (g) environment for relatively short duration exposures at bench scale. In recent years, efforts have focused on scaling up the electrolytic reduction process to assess its potential commercial application. Thus, the viability of platinum as an enduring inert anode in a large-scale process has come under increased scrutiny. Indeed, researchers have identified the degradation of platinum during the electrolytic reduction of uranium oxide via the formation of lithium platinate (Li_2PtO_3) and its subsequent disintegration [11-13]. Furthermore, the degradation of platinum is compounded in this system, as fission products from used fuel accumulate in the electrolyte and interact with platinum. Of particular concern are reactive fission products, such as iodine and tellurium, which accumulate as anions in the molten electrolyte and compete with oxygen anions for oxidation at the platinum anode [9-10]. Consequently, developmental efforts have ensued to investigate other potential inert anode materials, which can exhibit improved performance characteristics compared to platinum in the prescribed electrolytic reduction system.

Iridium, another platinum group metal, displays comparable thermodynamic stabilities to those shown by platinum in a LiCl-Li_2O-O_2 (g) system at 650 ° [14]. Additionally, iridium is less susceptible than platinum to interaction with lithium metal [15], which is formed during the electrolytic reduction process. However, to unequivocally compare performance characteristics, both monolithic platinum and iridium were operated as oxygen evolving anodes in the prescribed electrolytic reduction system. A series of uranium oxide reduction experiments was performed with both anodes operating simultaneously, positioned side-by-side against a common cathode. The anodes were subsequently subjected to a series of chemical and microscopic analyses to compare their performance characteristics.

2 Experimental

2.1 Equipment

The electrolytic reduction experiments were performed in an argon atmosphere radiological glovebox, in which a thermal well was located for molten salt operations. Equipment specific to the runs included four single-use cathode assemblies, two reusable anode assemblies (one with a platinum-tipped anode and the other with an iridium tip), and one Ni/NiO reference electrode, as shown in Fig. 1.

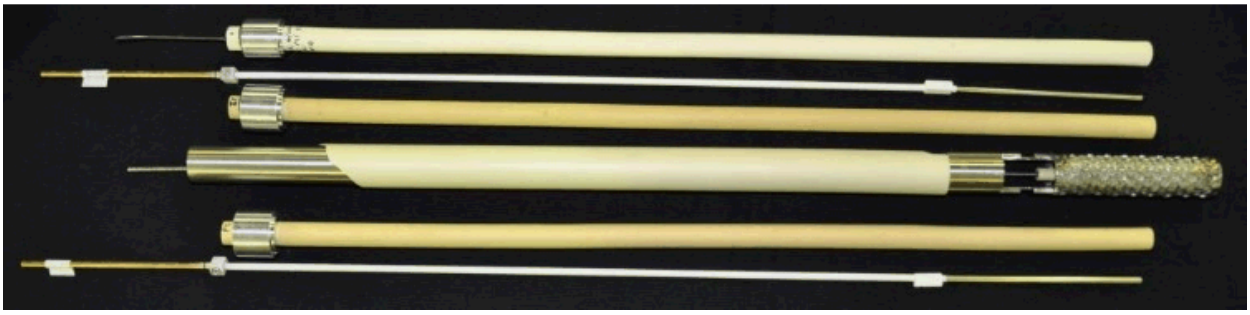

Fig. 1. Components used in the electrolytic reduction runs (from top to bottom): Ni/NiO reference electrode, iridium anode with its corresponding shroud, cathode assembly, and platinum anode with its corresponding shroud.

Each cathode assembly consisted of a stainless steel basket that was electrically isolated from a cathode rod or current collector. Each basket was fabricated by rolling and seam welding a prefabricated, multilayered, stainless steel mesh laminate of varying porosities (Purolator, 10 to 40 μm porosities) into a 19-mm diameter by 76-mm tall

cylinder. The bottom end of the cylinder was fitted with a solid end cap, and the upper end was fitted with an extension tube of the same diameter. The extension tube was sheathed with an alumina tube to provide electrical isolation from heat shields in the molten salt furnace. The upper end of the extension tube was fitted with a shaft collar to suspend the baskets at a prescribed position in the molten salt. The lower end of the extension tube was machined with openings to facilitate loading of the baskets with crushed uranium oxide particulate. Cathode rods were assembled with a 6-mm diameter by 38-mm tall stainless steel rod that was threaded onto a 3-mm diameter steel rod. A 6-mm diameter by 38-mm tall magnesia tube was placed concentric to the 3-mm diameter steel rod and atop the 6-mm diameter stainless steel rod to span the salt-gas interface when suspended in the salt pool. The cathode rods were positioned concentric to the cylindrical basket assemblies in such a way that each cathode rod was suspended about 6 mm off the bottom of the basket. Ceramic spacers and a polymeric shoulder disc were fitted onto the 3-mm diameter steel rod to electrically isolate the cathode rod from the basket assembly.

Each anode assembly consisted of a 100-mm long by 3-mm diameter monolithic platinum (99.8%, Alfa Aesar) or iridium (99.8%, Alfa Aesar) rod, which was coupled to a 3-mm diameter copper rod. (Note: After the first of four electrolytic reduction runs, the copper extension rods were replaced with 4-mm diameter nickel extension rods as a precautionary measure, due to observed corrosion on the surface of each copper rod. The surface corrosion was considered inconsequential to the performance of the respective platinum and iridium anodes.) Each anode rod was suspended inside an 11-mm OD by 8-mm ID magnesia tube by a shaft collar that positioned the bottom of each anode rod approximately 3 mm above the bottom opening of the magnesia tube.

The Ni/NiO reference electrode was comprised of a 1-mm diameter nickel wire in contact with 1 g of NiO powder inside a one-end closed magnesia tube with a porous end plug. The magnesia tube was fitted with a shaft collar to suspend the bottom end of the reference electrode in the molten salt.

2.2 Procedure

A 100-mm diameter by 110-mm tall magnesia crucible (Tateho Ozark Technical Ceramics) was loaded with 800 g of anhydrous LiCl (99.9%, ultra-dry, Alfa Aesar) and 8 g of Li_2O (99.5%, Alfa Aesar) for the first electrolytic reduction run. The crucible was placed inside the molten salt furnace well, and a vessel head with accompanying heat shields were positioned above the crucible. The vessel head and heat shields were aligned with five operating ports – one on center and four around the center – to access the molten salt electrolyte in the crucible. The Ni/NiO reference electrode was placed in one of two rear ports, and an ungrounded thermocouple assembly was placed in the other rear port. The platinum and iridium anode assemblies were placed in the front two ports, and a shield plug was placed in the center port. The furnace was energized and controlled to melt and maintain the salt pool at 650 ± 5 °C.

A cathode basket assembly, containing 25 g of uranium oxide of a specified particle size range, was positioned in the center port, suspending the loaded basket in the molten salt. Each anode was connected to the common cathode rod in the uranium oxide loaded basket through a separate Kepco bipolar operational power supply (BOP 20-10M). Each power supply was capable of ±10 A and ±20 VDC. The anode, cathode, reference electrode, and thermocouple leads were connected to an instrumentation and control cabinet, which provided furnace controls and electrochemical cell monitoring, i.e., anode and cathode currents and potentials relative to the Ni/NiO reference electrode. A simplified schematic of the ungrounded electrolytic reduction cell is shown in Fig. 2.

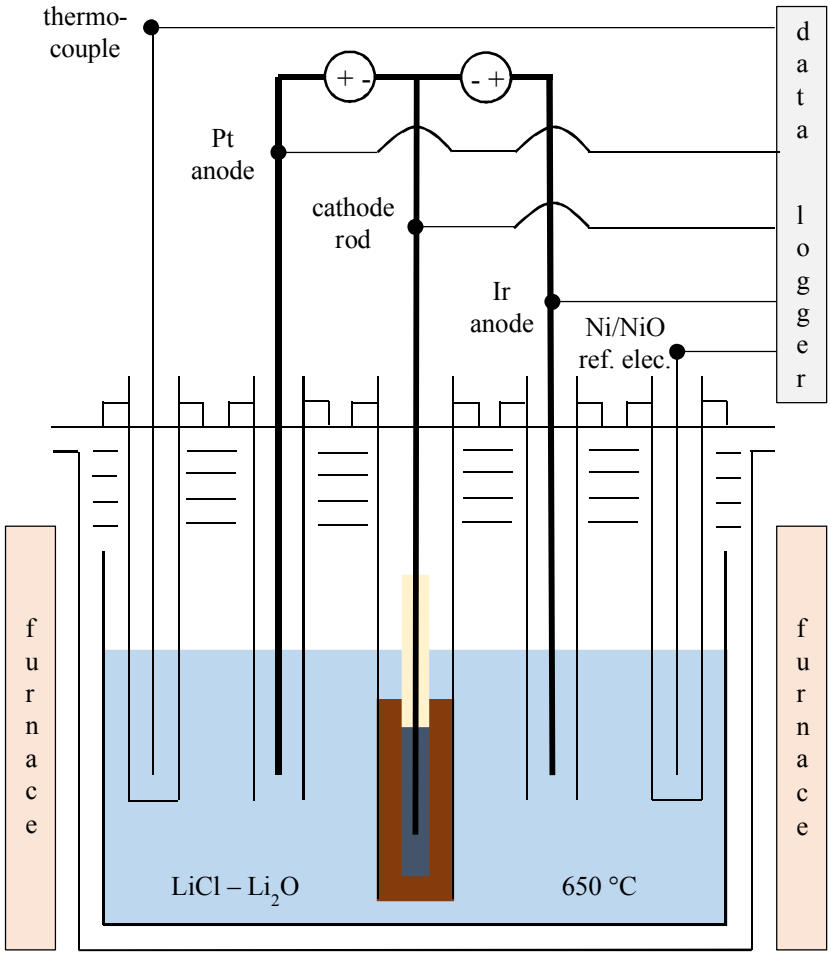

Fig. 2. Simplified diagram of the electrolytic reduction cell.

For a given run, both power supplies were simultaneously energized, stepped from an open circuit potential, and controlled at a 3.1 V cell voltage for ~15% of the theoretical charge for the loaded mass of uranium oxide (i.e., 35,700 C for 25 g UO_2), based on the observed currents through the anodes. (Note: The controlled 3.1 V cell voltage provided adequate overpotential to drive the decomposition of UO_2, which has a decomposition potential of 2.40 V at 650 °C. [14]) After ~5360 C of applied charge (one power cycle), both power supplies were de-energized for 30 minutes (one interrupt cycle) to facilitate oxygen ion diffusion from the basket to the bulk salt. Nine additional power and interrupt cycles were then performed, using the same cell voltage settings and durations as those established in the first cycles with the exception of one overnight period (i.e., extended interrupt cycle) per run. After the tenth power cycle the basket was allowed to sit at open circuit potential for 90 minutes, after which it was removed from the salt pool. A sample of the molten salt was taken, and the level of the salt pool was measured. The sample was dissolved in water and titrated, revealing the lithium oxide concentration in the salt. Masses of LiCl and Li_2O feedstock were prepared and added to the salt pool to restore salt level to its original level and Li_2O concentration to 1 wt%. A new cathode assembly was loaded with UO_2 particles, and the prescribed electrolytic reduction run sequence was repeated for three additional runs. The electrical leads to the platinum and iridium anodes were switched for the fourth run to assess possible differences between the performances of the two power supplies. A matrix of parameters for the series of four electrolytic reduction runs is presented in Table 1.

Table 1. Matrix of parameters for series of four electrolytic reduction runs.

Run	Cathode			Anode	
	UO_2 particulate mass	**UO_2 particulate size**	**Basket wall porosity**	**Power supply unit 1**	**Power supply unit 2**
1	25.0 g	0.045 – 1.2 mm	38 μm	Pt	Ir
2	25.0 g	0.045 – 1.2 mm	40 μm	Pt	Ir
3	25.0 g	0.045 – 1.2 mm	10 μm	Pt	Ir
4	25.0 g	< 0.045 mm	10 μm	Ir	Pt

2.3 Evaluation and Characterization of Anodes

The diameters of the post-test platinum and iridium anodes rods were measured with a slide caliper. Surface material from the rods was removed and examined by powder XRD (Panalytical Empyrean diffractometer, equipped with a Cu Kα target at 45 kV and 40 mA. A PIXcel^{3D} position-sensitive detector was used to collect the diffraction patterns. Scan parameters were 10–90° 2θ with a step of 0.013° 2θ and a scan step time of 198.6 s. Panalytical HighScore+ software was used to identify crystalline phases). Sections of the anode rods were examined under a scanning electron microscope (SEM) for morphological features (Phenom Pro SEM – NanoScience Instruments – with backscattered and energy dispersive detectors).

3 Results

3.1 Electrolytic Reduction

A response plot for the first electrolytic reduction run is shown in Fig. 3. The first power cycle in this run yielded platinum and iridium currents near 0.7 and 1.0 A, respectively. Over the course of the run those currents gradually approached each other, yielding 0.85 A each during the final power cycle. The first run was terminated after a total of 54,200 C of total charge (or 152% of theoretical charge) was applied, with the platinum and iridium anodes carrying 43.2% and 56.8% of the total charge, respectively.

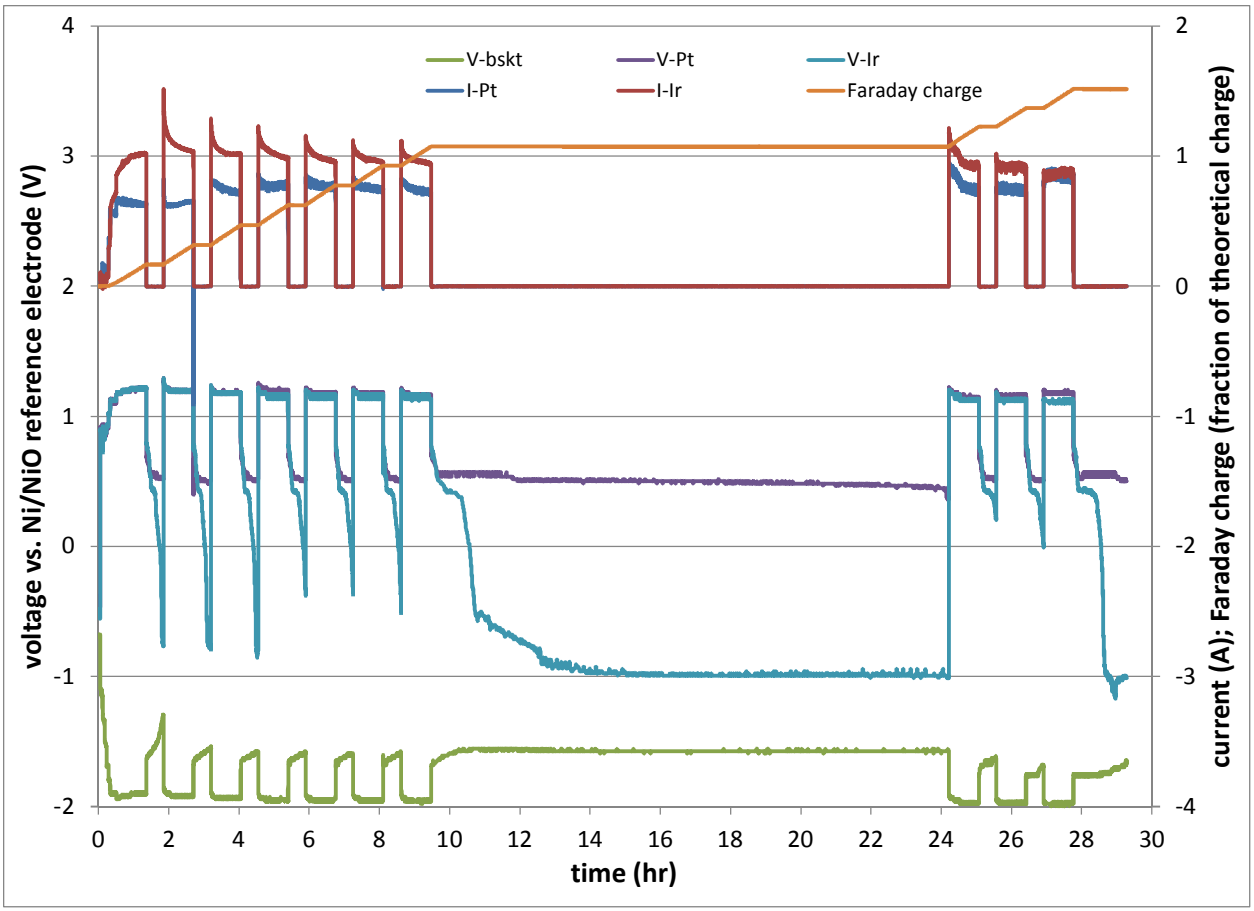

Fig. 3. Response plot for first electrolytic reduction run.

The second electrolytic reduction run proceeded in a similar fashion to that of the first run, yielding a response plot with the platinum anode carrying 41.8% of the total applied charge versus 58.2% for iridium. The third and fourth electrolytic reduction runs likewise produced similar response plots to the first two runs, with the exception that the platinum and iridium currents exhibited more parity throughout their respective runs. Indeed, the swapping of power supplies between the platinum and iridium anodes during the fourth run identified no perceptible difference in anode current carrying capacities. A summary of the charges for the series of four electrolytic reduction runs is provided in Table 2.

Table 2. Summary of charges for series of electrolytic reduction runs.

Run	Theoretical Charge (C)	Total Applied Charge (Pt and Ir)		Anode Specific Charge			
				Pt		Ir	
		Actual charge (C)	Fraction of theoretical charge (%)	Charge (C)	Fraction of total charge (%)	Charge (C)	Fraction of total charge (%)
1	35,700	54,200	152	23,400	43.2	30,800	56.8
2	35,700	58,600	164	24,500	41.8	34,100	58.2
3	35,700	59,000	165	31,200	52.9	27,800	47.1
4	35,700	53,700	150	28,700	53.4	25,000	46.6
Totals	142,800	225,500	158	107,800	47.8	117,700	52.2

3.2 Evaluation of Anodes

After the series of four electrolytic reduction runs, the platinum and iridium anodes were removed from the molten salt furnace, allowed to cool to room temperature, and then soaked in deionized water to remove adhered salt. The physical states of the cleaned anode rods are shown in Fig. 4. As observed in Fig. 4, the iridium anode rod surface looked uniformly dark and smooth, and no thinning of the rod was visually apparent. The platinum anode rod exhibited a yellow-green surface material in the region above the salt level, while the surface in contact with the salt was rough and of a dull-gray color. The platinum anode rod looked somewhat thinner in the region below the salt level.

Fig. 4. Iridium (top) and platinum (bottom) anode rods after water washing.

A slide caliper was used to measure the diameters of both platinum and iridium anode rods at 10 mm increments, beginning from the bottom end of each rod. The results of these measurements are shown in Table 3. The calipers were also used to measure from the bottom end of the platinum anode rod to the onset of the yellow-green surface deposits, which was likely the salt-gas interface during the runs. The distance was 46 mm.

Table 3. Diameters over the lengths of platinum and iridium rods after series of four electrolytic reduction runs.

Distance from bottom end of each anode rod (mm)	**Diameter of anode rod (mm)**	
	Pt	**Ir**
0	2.87	2.97
10	2.73	2.97
20	2.60	2.96
30	2.52	2.96
40	2.63	2.97
50	2.82	2.98
60	2.94	2.98
70	2.97	2.97
80	2.96	2.97

A straight edge was used to scrape material from the surface of the platinum anode rod, which consisted predominantly of the yellow-green surface material on the upper portion of the rod. The same scraping was attempted on the iridium anode rod, but very little material could be removed. The scraped materials from both anode rods were examined by powder XRD. Electron discharge machining was then used to section the bottom 3 millimeters of each rod, which were subsequently mounted in epoxy, polished, and examined with a SEM.

Figs. 5 and 6 show the diffraction patterns of the platinum and iridium anode surface materials, respectively. Two phases that were identified from the scraped platinum material matched metallic platinum and lithium platinate (Li_2PtO_3). The phase identification of the iridium anode surface material was less conclusive, due to the very small quantity of sample that could be collected. The XRD pattern revealed the presence of trace iridium metal along with a second phase, which could not be conclusively established as lithium iridate or iridium oxide (Li_2IrO_3, IrO_2). The

presence of trace platinum and iridium metal in the XRD patterns was believed to be due to the scraping of the respective anode rods with a straight edge.

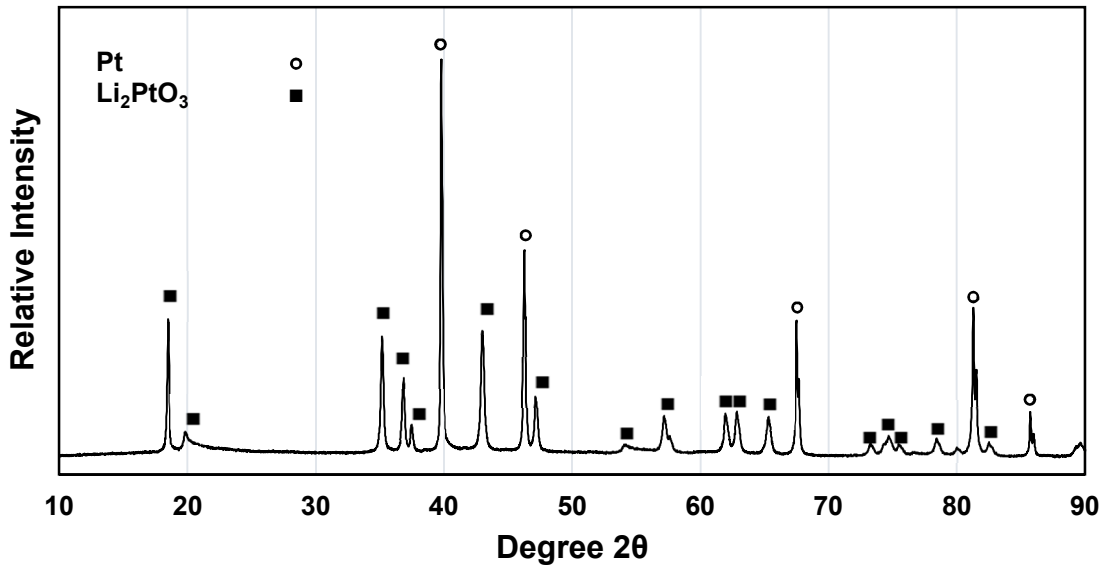

Fig. 5. X-ray diffraction pattern from platinum rod surface material showing Li_2PtO_3 and Pt metal.

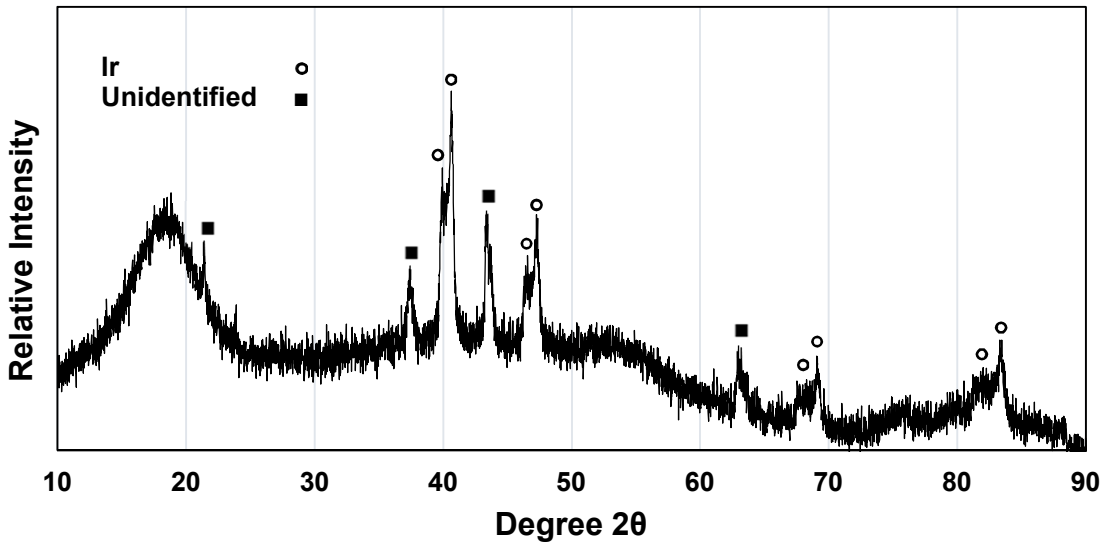

Fig. 6. Iridium rod surface material XRD pattern showing a pattern match to Ir metal but an uncertain match to Li_2IrO_3 or IrO_2.

Images of the bottom sections (3 mm) of the platinum and iridium anode rods are shown in Figs. 7 and 8, respectively. The images did not reveal the presence of any corrosion layers, even up to a magnification of 10,000x. There could be two possibilities for the absence of a corrosion layer, particularly in the Pt sample, either the corrosion layer was removed during the sample preparation, or, if present, it did not provide enough imaging contrast to distinguish it from the bulk metal. Subsequent Energy Dispersion Spectroscopy (EDS) could not distinguish a corrosion layer on either sample, because lithium cannot be detected by the EDS spectrometer and also the adjacent epoxide from the mounted samples prevented an accurate observation of oxygen, conclusively from a corrosion layer. However, the SEM images qualitatively identified a more roughened surface on the platinum anode rod (Fig. 7 with increasing magnification) as opposed to the surface of the iridium anode rod (Fig. 8).

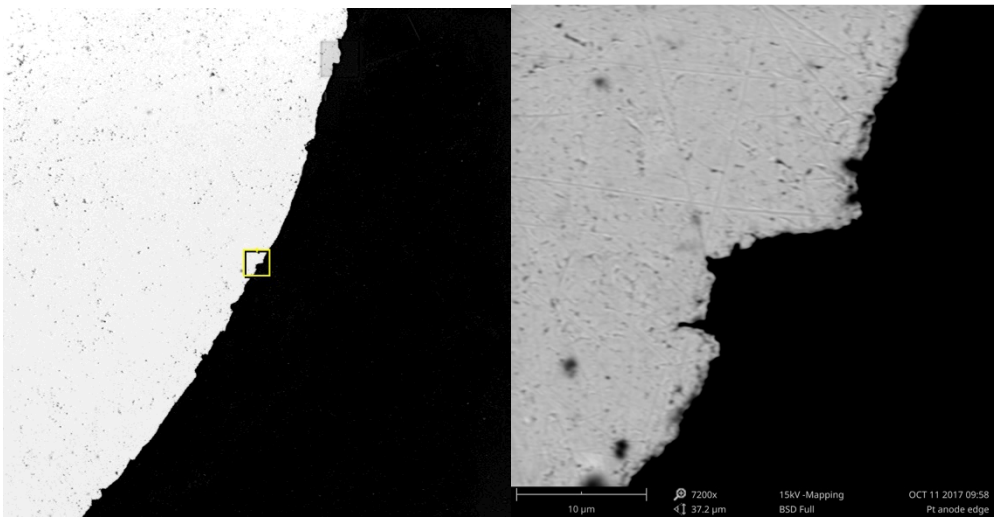

Fig. 7. Edge of platinum anode at low magnification (left) and high magnification (right).

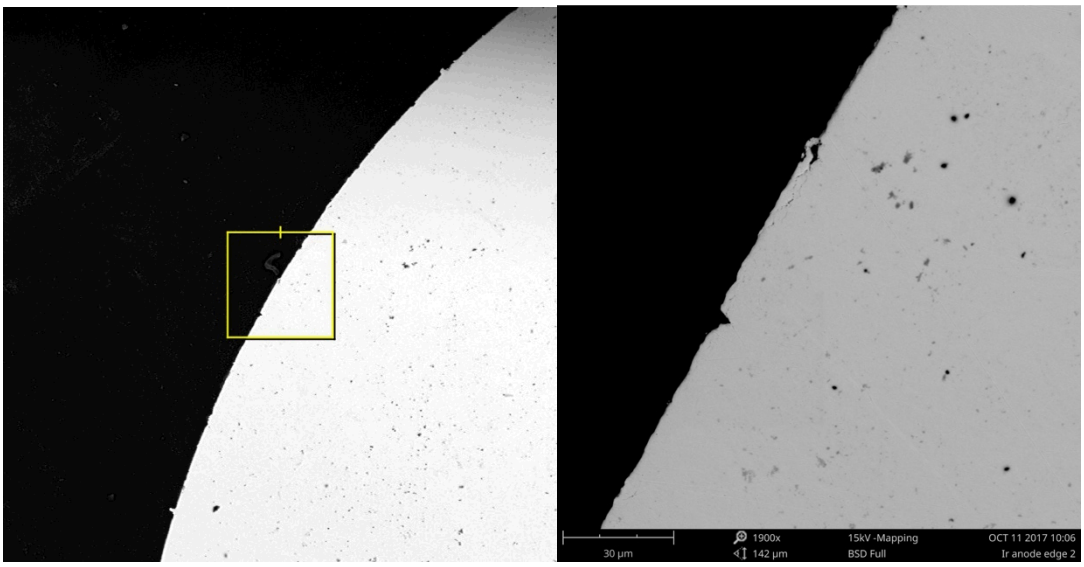

Fig. 8. Edge of iridium anode at low magnification (left) and high magnification (right).

4 Discussion

This study was designed to compare the performance of monolithic platinum vis-à-vis iridium anodes under identical operating conditions during the electrolytic reduction of uranium oxide with independent power supplies. One possible discriminator in terms of performance was the current and charge carried by each anode. In the first run, the initial current on a clean iridium anode was nearly 50% higher than that for a clean platinum anode, as shown in Fig. 3, owing to a higher electrical conductivity of pure iridium than that of pure platinum. However, the platinum and iridium anode currents gradually approached each other over the course of the first run, which is likely due to compound formations and concomitant changes in conductivity at the salt-metal interface of each anode. Indeed, the anode specific charges for the two anodes were comparable over the series of four runs with platinum carrying 47.8% of the applied charge and iridium carrying 52.2%. Thus, the relative conductivities of platinum and iridium were not a substantial discriminator between the two anode materials, particularly after an initial period of surface conditioning.

Platinum forms an oxide layer of lithium platinate, Li_2PtO_3, when operating as an anode in the electrolytic reduction system. The formation of lithium platinate in this system has been observed consistently by others [11-13]. Indeed, lithium platinate was the major species on the platinum anode surface identified in this study via powder XRD. Researchers have observed Li_2PtO_3 formation at temperatures above 600 °C [16], exhibiting a yellow polycrystalline growth [17], which is consistent with the yellow-green surface formation on the platinum anode at 650 °C in this study. In contrast, Freund identified lithium iridate, Li_2IrO_3, formation above 700 °C [17], which had been characterized as black crystals previously by others [18]. Several authors have reported the formation of three types of lithium iridates (α-Li_2IrO_3, β-Li_2IrO_3, and γ-Li_2IrO_3). Kobayashi, et al, were the first to report the synthesis of a polycrystalline α-Li_2IrO_3 by heating mixtures of Li_2CO_3 and IrO_2 to temperatures between 650 and 1050 °C [19]. Takayama, et al, have reported that α-Li_2IrO_3 becomes irreversibly converted to β-Li_2IrO_3 upon repetitive heating at a temperature higher than 1000 °C [20]. According to Freund, et al [17], the formation of α-Li_2IrO_3 takes place in the temperature range of 750 – 1050 °C. Modic, et al, prepared γ-Li_2IrO_3 by a combination of calcination and molten salt annealing of Li_2CO_3 and IrO_2 mixture in molten LiOH at 700 °C to 800 °C [21]. From a conductivity standpoint, it has been reported that while Li_2PtO_3 is a semiconductor with an energy band gap of 2.3 eV, Li_2IrO_3 exhibits metallic conductivity [18]. Although the present study identified an extremely thin black formation on the surface of the iridium anode, the presence of Li_2IrO_3 was inconclusive due to its insufficient formation and obtainability on the iridium anode surface for subsequent analysis. Perhaps the lack of significant Li_2IrO_3 formation on the iridium anode was attributable to the lower operating temperature (650 °C) in this study compared to Li_2IrO_3 crystal growth by others at temperatures above 700 °C.

The most persuasive discriminator in this study was the mechanical stability of the anode materials and their corresponding surface formations. The initial diameters of the platinum and iridium rods were 3 mm. However, over the course of the four electrolytic reduction runs, the platinum exhibited a significantly higher material loss compared to iridium (Table 3). This difference in anode material losses is accentuated in a radial profile plot, as shown in Fig. 9. The loss of anode material, or necking, corresponded to a reduction in cross-sectional area as high as 29% for the platinum rod compared to 3% for iridium.

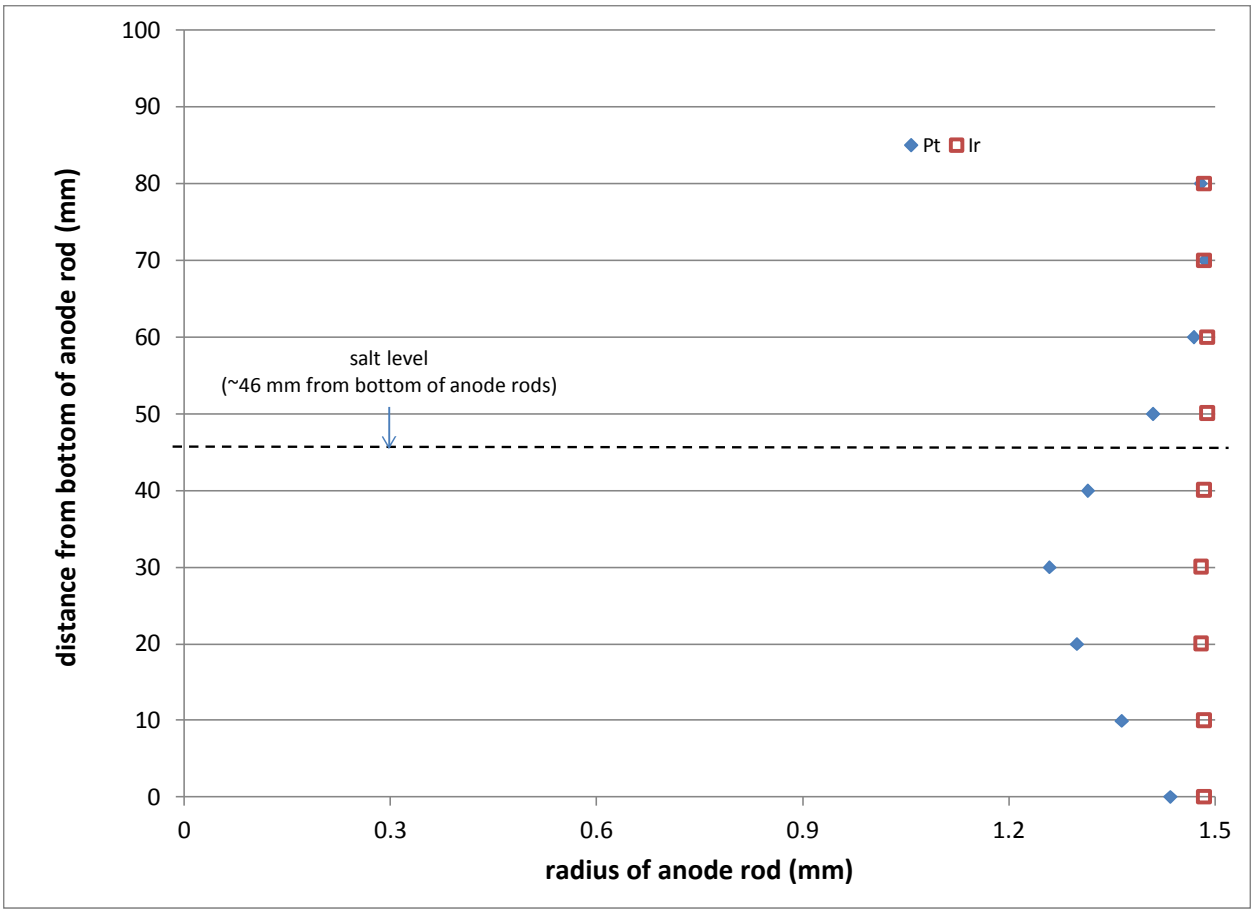

Fig. 9. Radial profiles of platinum and iridium anode rods following series of four electrolytic reduction runs.

Both platinum and iridium anode rods exhibited surface formations. However, the formation of Li_2PtO_3 on the platinum surface proved unstable, becoming progressively thinner from the bottom of the rod towards the salt-gas interface. The progressive thinning of the platinum rod could be attributed to a Li_2O concentration gradient that was suspected in the column of salt inside the anode shroud. Specifically, the lithium oxide concentration at the bottom of the anode shroud opening should have been near that in the bulk salt, while its concentration should have gradually lowered moving up the column of salt within the shroud due to oxygen anion oxidation on the anode. Jeong, et al., noted that platinum degradation was accelerated at low Li_2O concentrations, particularly below 0.5 wt% [12], which is consistent with the thinning of the platinum anode rod in this study. The progressive thinning of the platinum anode rod and consequent exposure of base platinum metal could explain the slightly higher charges that were observed during the third and fourth runs (see Table 2). The iridium anode rod, on the other hand, exhibited a stable surface formation, in spite of a similarly suspected Li_2O concentration gradient in the column of salt within its respective anode shroud.

5 Conclusions

This study provided compelling evidence that monolithic iridium exhibited superior performance characteristics vis-à-vis platinum during the electrolytic reduction of uranium oxide in LiCl – 1 wt% Li_2O at 650 °C. Both platinum and iridium anodes were effective at removing oxygen anions from the molten salt electrolyte. The platinum anode carried 47.8% of the applied charge from a series of four electrolytic reduction runs, while the iridium anode carried the balance of the charge. Both anode rods exhibited surface formations. The platinum anode rod formed a yellow-green surface layer, which was characterized to be Li_2PtO_3 via powder XRD. The iridium anode rod formed a

smooth dark surface layer. The color of the iridium surface was consistent with Li_2IrO_3; however, its formation could not be conclusively established, because of its insufficient buildup on the anode surface. The primary discriminator in this comparative study was the stability of the anode surface layers. The platinum anode rod degraded in this system via Li_2PtO_3 formation and erosion, resulting in its thinning up to 29% of its original cross-sectional area. The iridium anode rod appeared to form a relatively stable conductive surface layer under identical conditions, and its thinning was no more than a 3% of the original cross-sectional area.

6 Acknowledgements

This work was supported by the U.S. Department of Energy (DOE), Office of Nuclear Energy, under DOE Idaho Operations Office contract DE-AC07-05ID14517.

7 References

1. Gourishankar K, Redey L, Williamson M (2002) Electrolytic Reduction of Metal Oxides in Molten Salts. In: Schneider W (ed) Light Metals 2002, The Minerals, Metals and Materials Society, Pennsylvania, pp 1075-1082
2. Goff KM, Wass JC, Marsden KC, Teske GM (2011) Electrochemical processing of used nuclear fuel. Nucl Eng Technol 43:335-342
3. Williamson MA, Willit JL (2011) Pyroprocessing flowsheets for recycling used nuclear fuel. Nuc Eng Technol 43:329-334
4. Inoue T, Koyama T, Arai Y (2011) State of the art of pyroprocessing technology in Japan. Energ Procedia 7:405-413
5. Sakamura Y, Omori T (2010) Electrolytic reduction and electrorefining of uranium to develop pyrochemical reprocessing of oxide fuels. Nucl Technol 171:266-275
6. Lee H, Park G-I, Kang K-H, Hur J-M, Kim J-G, Ahn D-H, Cho Y-Z, Kim EH (2011) Pyroprocessing technology development at KAERI. Nucl Eng Technol 43:317-328
7. Choi E-Y, Jeong SM (2015) Electrochemical processing of spent nuclear fuels: An overview of oxide reduction in pyroprocessing technology. Prog Nat Sci-Mater 25: 572-582
8. Nagarajan K, Reddy BP, Ghosh S, Ravisankar G, Mohandas KS, Mudali UK, Kutty KVG, Viswanathan K, Babu CA, Kalyanasundaram P, Rao PRV, Raj B (2011) Development of Pyrochemical Reprocessing for Spent Metal Fuels. Energ Procedia 7:431-436
9. Herrmann SD, Li SX (2010) Separation and recovery of uranium metal from spent light water reactor fuel via electrolytic reduction and electrorefining. Nucl Technol 171:247-265
10. Herrmann SD, Li SX, Westphal BR (2012) Separation and recovery of uranium and group actinide products from irradiated fast reactor MOX fuel via electrolytic reduction and electrorefining. Sep Sci Technol 47:2044-2059
11. Sakamura Y, Kurata M, Inoue T (2006) Electrochemical reduction of UO_2 in molten $CaCl_2$ or LiCl. J Electrochem Soc 153(3):d31-d39
12. Jeong SM, Shin H-S, Cho S-H, Hur J-M, Lee HS (2009) Electrochemical behavior of a platinum anode for reduction of uranium oxide in a LiCl molten salt. Electrochim Acta 54:6335-6340

13. Lee S-K, Jeon MK, Kim S-W, Choi E-Y, Lee J, Hong S-S, Oh S-C, Hur J-M (2018) Evaluation of Pt anode stability in repeated electrochemical oxide reduction reactions for pyroprocessing. J Radioanal Nucl Ch 316:1053-1058

14. Outotec (2015) HSC Chemistry 8. Pori, Finland.

15. ASM International (2016) ASM Alloy Phase Diagram Database. Villars P (ed) https://matdata.asminternational.org/apd/index.aspx

16. Kasuyu R, Miki T, Morikawa H, Tai Y (2013) Synthesis of alkali metal platinates and their dissolution behavior in hydrochloric acid. J Ceram Soc Jpn 121(10):884-890

17. Freund F, Williams SC, Johnson RD, Coldea R, Gegenwart P, Jesche A (2016) Single crystal growth from separated educts and its application to lithium transition-metal oxides. Sci Rep [6:35362] DOI: 10.1038/srep35362

18. O'Malley MJ, Verweij H, Woodward PM (2008) Structure and properties of ordered Li_2IrO_3 and Li_2PtO_3. J Solid State Chem 181:1803-1809

19. Kobayashi H, Kanno R, Tabuchi M, Kageyama H, Nakamura O, Takano M (1997) Structure and charge/discharge characteristics of new layered oxides: $Li_{1.8}Ru_{0.6}Fe_{0.6}O_3$ and Li_2IrO_3. J Power Sources 68:686-691

20. Takayama T, Kato A, Dinnebier R, Nuss J, Kono H, Veiga LSI, Fabbris G, Haskel D, Takagi H (2015) Hyperhoneycomb iridate β-Li_2IrO_3 as a platform for Kitaev magnetism. Phys Rev Lett 114, 077202:1-5

21. Modic KA, Smidt TE, Kimchi I, Breznay NP, Biffin A, Choi S, Johnson RD, Coldea R, Watkins-Curry P, McCandless GT, Chan JY, Gandara F, Islam Z, Vishwanath A, Shekhter A, McDonald RD, Analytis JG (2014) Realization of a three-dimensional spin-anisotropic harmonic honeycomb iridate. Nat Commun [5:4203] DOI: 10.1038/ncomms5203